bioRxiv preprint doi: https://doi.org/10.1101/2023.09.25.559399; this version posted September 27, 2023. The copyright holder for this preprint (which was not certified by peer review) is the author/funder. All rights reserved. No reuse allowed without permission.

Axon morphology and intrinsic cellular properties determine repetitive transcranial magnetic stimulation threshold for plasticity

Christos Galanis[1], Lena Neuhaus[1], Nicholas Hananeia[2], Zsolt Turi[1], Peter Jedlicka[2], Andreas Vlachos[1, 3, 4]

[1]Department of Neuroanatomy, Institute of Anatomy and Cell Biology, Faculty of Medicine, University of Freiburg, Freiburg, Germany

[2]3R-Zentrum Gießen, Justus-Liebig-Universitat Giessen, Giessen, Germany

[3] Center BrainLinks-BrainTools, University of Freiburg, Freiburg, Germany

[4] Center for Basics in NeuroModulation (NeuroModulBasics), Faculty of Medicine, University of Freiburg, Freiburg, Germany

Correspondence to vlachos@anat.uni-freiburg.de
Department of Neuroanatomy,
Institute of Anatomy and Cell Biology,
Faculty of Medicine,
University of Freiburg,
Freiburg 79104,Germany

Keywords: synaptic plasticity, morphology,axons, inhibition, excitation, whole-cell patch-clamp recordings, organotypic tissue cultures.

Running title: Neuronal morphology and rTMS

Figures: 8, Pages: 31, Words in abstract: 287, Introduction: 617, Discussion: 1509

Acknowledgements: We thank Susanna Glaser for skillful assistance in tissue culturing. The work was supported by National Institutes of Health, USA (NIH; 1R01NS109498) and by the Federal Ministry of Education and Research, Germany (BMBF, 01GQ2205A)

bioRxiv preprint doi: https://doi.org/10.1101/2023.09.25.559399; this version posted September 27, 2023. The copyright holder for this preprint (which was not certified by peer review) is the author/funder. All rights reserved. No reuse allowed without permission.

Abstract

Repetitive transcranial magnetic stimulation (rTMS) is a widely used therapeutic tool in neurology and psychiatry, but its cellular and molecular mechanisms are not fully understood. Standardizing stimulus parameters, specifically electric field strength and direction, is crucial in experimental and clinical settings. It enables meaningful comparisons across studies and facilitating the translation of findings into clinical practice. However, the impact of biophysical properties inherent to the stimulated neurons and networks on the outcome of rTMS protocols remains not well understood. Consequently, achieving standardization of biological effects across different brain regions and subjects poses a significant challenge. This study compared the effects of 10 Hz repetitive magnetic stimulation (rMS) in entorhino-hippocampal tissue cultures from mice and rats, providing insights into the impact of the same stimulation protocol on similar neuronal networks under standardized conditions. We observed the previously described plastic changes in excitatory and inhibitory synaptic strength of CA1 pyramidal neurons in both mouse and rat tissue cultures, but a higher stimulation intensity was required for the induction of rMS-induced synaptic plasticity in rat tissue cultures. Through systematic comparison of neuronal structural and functional properties and computational modeling, we found that morphological parameters of CA1 pyramidal neurons alone are insufficient to explain the observed differences between the groups. However, axon morphologies of individual cells played a significant role in determining activation thresholds. Notably, differences in intrinsic cellular properties were sufficient to account for the 10 % higher intensity required for the induction of synaptic plasticity in the rat tissue cultures. These findings demonstrate the critical importance of axon morphology and intrinsic cellular properties in predicting the plasticity effects of rTMS, carrying valuable implications for the development of computer models aimed at predicting and standardizing the biological effects of rTMS.

bioRxiv preprint doi: https://doi.org/10.1101/2023.09.25.559399; this version posted September 27, 2023. The copyright holder for this preprint (which was not certified by peer review) is the author/funder. All rights reserved. No reuse allowed without permission.

INTRODUCTION

Repetitive transcranial magnetic stimulation (rTMS) is a non-invasive technique that modulates cortical excitability beyond the stimulation period (Chen et al., 1997; Huang et al., 2005; Suppa et al., 2016). Despite its increasing use for treating neuropsychiatric disorders such as major depression (Cocchi et al., 2018; Garnaat et al., 2018; Rehn et al., 2018; Voigt et al., 2019; Somaa et al., 2022), the cellular and molecular mechanisms of rTMS in human cortical networks remain not well understood (Müller-Dahlhaus and Vlachos, 2013; Cirillo et al., 2017). Animal models, both *in vivo* and *in vitro*, have provided important insights into mechanisms by which rTMS modifies neuronal circuit excitability and plasticity (Vlachos et al., 2012; Tokay et al., 2014; Lenz et al., 2016; Hong et al., 2020; Romero et al., 2022; Eichler et al., 2023). It has been shown for example that rTMS affects the functional and structural properties of excitatory and inhibitory synapses (Tokay et al., 2009; Vlachos et al., 2012; Lenz et al., 2016), and that it facilitates the reorganisation of abnormal cortical circuits (Tang et al., 2021; Moretti et al., 2022). Recently, experimental evidence for an involvement of microglia, the brains resident immune cells in rTMS-induced synaptic plasticity was provided (Eichler et al., 2023).

Although rTMS has shown robust neurobiological effects in animal models, its efficacy in humans varies significantly (Goldsworthy et al., 2014; López-Alonso et al., 2014; Vallence et al., 2015; Guerra et al., 2020) due to challenges in dose standardization, among others (Peterchev et al., 2012; Turi et al., 2021). Considerable effort has been made to standardize the electric field strength across brain regions and subjects to improve reproducibility and better understand the effects of single pulse and rTMS across brain regions (Opitz et al., 2011; Thielscher et al., 2011; Saturnino et al., 2019). Meanwhile, it is becoming increasingly clear that computational models that predict the strength and orientation of TMS-induced electric field must be extended to biological effects (c.f., Turi et al., 2022), i.e., the electric fields must be coupled to biophysically

bioRxiv preprint doi: https://doi.org/10.1101/2023.09.25.559399; this version posted September 27, 2023. The copyright holder for this preprint (which was not certified by peer review) is the author/funder. All rights reserved. No reuse allowed without permission.

realistic models (Aberra et al., 2018; Shirinpour et al., 2021). Indeed, these computational approaches provided important insight into the role of neuronal morphologies, specifically axons and myelination, which seem to play a critical role for single pulse TMS (Aberra et al., 2020). Although some attempts have been made to compute rTMS-induced changes in intracellular calcium levels, which could be used to predict plasticity effects (Shirinpour et al., 2021), our knowledge regarding dose-response interrelation of rTMS-induced synaptic plasticity is limited. As a consequence, it is currently also not possible to compute and standardize synaptic plasticity induction across brain regions and subjects.

In this study, we investigated the after effects of 10 Hz repetitive magnetic stimulation (rMS) and explored how structural, electrophysiological, and network properties may influence the plasticity response of neurons. To this end we employed a cross-species strategy to compare seemingly similar neurons and networks and studied the effects of rMS in mouse and rat entorhino-hippocampal slice cultures. Notably, we discovered that a 10% stronger intensity, i.e., maximum stimulator output (MSO), was required to induce plasticity in rat CA1 pyramidal neurons compared to their mouse counterparts. To address this discrepancy, we examined various factors, including the structural characteristics of the neurons, their electrophysiological properties, and the network dynamics within which they operate. By thoroughly investigating these elements, we aimed to uncover the mechanisms underlying the differential responsiveness of rat and mouse CA1 pyramidal neurons to 10 Hz rMS. Our findings provide new insights into the cellular determinants that govern the plasticity outcomes of rTMS and shed light on the factors influencing the effectiveness of the stimulation, with important consequences for the standardisation of biological dose in comparable neuronal networks within and across subjects.

bioRxiv preprint doi: https://doi.org/10.1101/2023.09.25.559399; this version posted September 27, 2023. The copyright holder for this preprint (which was not certified by peer review) is the author/funder. All rights reserved. No reuse allowed without permission.

MATERIALS AND METHODS

Ethics statement: Mice and rats were maintained in a 12-hour light/dark cycle with food and water ad libitum. Every effort to minimize the distress and pain of animals was made. All experimental procedures were performed according to the German animal welfare legislation, approved by the appropriate animal welfare committee and the animal welfare officer of the University of Freiburg.

Animals: Mice of the strain C57BL6/J and rats of the strain Wistar (Crl:WI) of both sexes were used in this study.

Preparation of organotypic entorhino-hippocampal tissue cultures: Organotypic tissue cultures containing the hippocampus and the entorhinal cortex were prepared at postnatal day 3-5 from mice and rats of either sex as described preciously (Galanis et al., 2021; Vlachos et al. 2012). The tissue cultures were maintained in an incubator at 35 °C with 5 % CO2 for at least 18 days before any experimental assesment. Tissue culture medium was changed 3 times per week and consisted of 50% (v/v) MEM, 25% (v/v) basal medium eagle (BME), 25% (v/v) heat-inactivated normal horse serum, 25 mm HEPES, 0.15% (w/v) NaHCO3, 0.65% (w/v) glucose, 0.1 mg/ml streptomycin, 100 U/ml penicillin, and 2 mm Glutamax (pH 7.3 with HCl or NaOH).

rMS in vitro: Tissue cultures were transferred in a standard 35 mm petri dish filled with standard extracellular solution (129 mM NaCl, 4 mM KCl, 1 mM MgCl2, 2 mM CaCl2, 4.2 mM glucose, 10 mM HEPES, 0.1 mg/ml streptomycin, 100 U/ml penicillin, pH 7.4; preheated to 35 °C; 365mOsm with sucrose). A standard 70-mm figure-of-eight coil (D70 Air Film Coil, Magstim) connected to a Magstim Super Rapid2 Plus1 (Magstim) was placed 1 mm above the lid of the petri dish and the cultures were stimulated with a protocol consisting of 900 pulses at 10 Hz. Tissue cultures were orientated in a way that the induced electric field within the tissue was approximately

bioRxiv preprint doi: https://doi.org/10.1101/2023.09.25.559399; this version posted September 27, 2023. The copyright holder for this preprint (which was not certified by peer review) is the author/funder. All rights reserved. No reuse allowed without permission.

parallel to the dendritic tree of CA1 pyramidal neurons. Different stimulation intensities (maximum stimulator output – MSO) were used in this study and are reported in each experiment respectively. Species-, age- and time-matched cultures were not stimulated, but otherwise treated identical to stimulated cultures served as the controls.

Whole-cell voltage-clamp recordings: Whole-cell voltage-clamp recordings of CA1 pyramidal cells were conducted at 35°C. The bath solution contained 126 mM NaCl, 2.5 mM KCl, 26 mM NaHCO3, 1.25 mM NaH2PO4, 2 mM CaCl2, 2 mM MgCl2, and 10 mM glucose and was saturated with 95% O2/5% CO2. A-amino-3-hydroxy-5-methyl-4-isoxazolepropionic acid (AMPA) receptor mediated miniature excitatory postsynaptic currents (mEPSCs) were recorded in the presence of 10 µM D-APV and 0.5 µM TTX in the bath solution while the patch pipettes contained 126 mM K-gluconate, 4 mM KCl, 4 mM ATP-Mg, 0.3 mM GTP-Na2, 10 mM PO-creatine, 10 mM HEPES, and 0.1% (w/v) biocytin (pH 7.25 with KOH, 290 mOsm with sucrose). Gamma-aminobutyric acid (GABA) receptor mediated miniature inhibitory post synaptic currents (mIPSCs) were recorded in the presence of 0.5 µM TTX, 10 µM D-APV, and 10 µM CNQX in the bath solution while the patch pipettes contained 125 mM CsCl, 5 mM NaCl, 2 mM MgCl2, 2 mM Mg-ATP, 0.5 mM Na2-GTP, 0.1 mM EGTA and 10 mM HEPES (pH=7.33 with CsOH; 275 mOsm with sucrose). Neurons were recorded at a holding potential of −70 mV. Series resistance was monitored in 2 - 4 min intervals and recordings were discarded if the series resistance reached ≥30 MΩ and the leak current changed significantly.

Whole-cell current-clamp recordings: Whole-cell current-clamp recordings of CA1 pyramidal cells were conducted at 35°C. The bath solution contained 126 mM NaCl, 2.5 mM KCl, 26 mM NaHCO3, 1.25 mM NaH2PO4, 2 mM CaCl2, 2 mM MgCl2, 10 mM glucose, 10 µM D-APV, 10 µM CNQX, and 10 µM bicuculline methiodide and was saturated with 95% O2/5% CO2. Patch

bioRxiv preprint doi: https://doi.org/10.1101/2023.09.25.559399; this version posted September 27, 2023. The copyright holder for this preprint (which was not certified by peer review) is the author/funder. All rights reserved. No reuse allowed without permission.

pipettes contained 126 mM K-gluconate, 4 mM KCl, 4 mM ATP-Mg, 0.3 mM GTP-Na2, 10 mM PO-creatine, 10 mM HEPES, and 0.1% (w/v) biocytin (pH 7.25 with KOH, 290 mOsm with sucrose). Neurons were hyperpolarized with −100 pA and then depolarized up to +400 pA with 1-s-long 10 pA current injection steps. Pipette capacitance was neutralized, bridge balance activated and series resistance was monitored before and after the recording of each cell. Recordings were discarded of the series resistance reached ≥15 MΩ.

High-density microelectrode array (HD-MEA) recordings: HD-MEA recordings of mouse and rat tissue cultures were conducted at 35°C. The bath solution contained 126 mM NaCl, 2.5 mM KCl, 26 mM NaHCO3, 1.25 mM NaH2PO4, 2 mM CaCl2, 2 mM MgCl2, 10 mM glucose and was saturated with 95% O2/5% CO2. Tissue cultures were placed on an Accura HD-MEA chip (3Brain, Switzerland) containing 4096 electrodes and left to acclimatize for 2 min before starting the experiment. Each tissue culture was recorded for 10 min with a BioCAM DupleX (3Brain, Switzerland).

Neuronal filling, post hoc staining and imaging: CA1 pyramidal neurons were patched with pipettes containing 126 mM K-gluconate, 4 mM KCl, 4 mM ATP-Mg, 0.3 mM GTP-Na2, 10 mM PO-creatine, 10 mM HEPES, and 1% (w/v) biocytin (pH 7.25 with KOH, 290 mOsm with sucrose). To achieve a comprehensive visualization of axonal morphologies, an elevated biocytin concentration was necessary. Only a single cell was filled within each culture, facilitating the clear identification of axons specific to that neuron. The neurons were kept in the whole-cell configuration for at least 10 min during which they were depolarized with 100 ms current injections of 200 pA at 5 Hz.. Tissue cultures were fixed in a solution of 4% (w/v) PFA and 4% (w/v) sucrose in 0.01 M PBS for 1 h. The fixed tissue was incubated for 1 h with 10% (v/v) NGS and 0.5% (v/v) Triton X-100 in 0.01 M PBS. Biocytin (Sigma Millipore, catalog #B4261) filled

bioRxiv preprint doi: https://doi.org/10.1101/2023.09.25.559399; this version posted September 27, 2023. The copyright holder for this preprint (which was not certified by peer review) is the author/funder. All rights reserved. No reuse allowed without permission.

cells were stained with Alexa488-conjugated streptavidin (Thermo Fisher Scientific; 1:1000; in 0.01 m PBS with 10% NGS and 0.1% Triton X-100) for 4 h, and DAPI (Thermo Fisher Scientific) staining was used to visualize cytoarchitecture (1:5000; in 0.01 m PBS for 15 min). Slices were washed, transferred, and mounted onto glass slides for visualization. Streptavidin-stained CA1 pyramidal neurons were visualized and multiple z-stacks (step size 0.5 μm) were obtained with a Leica Microsystems TCS SP8 laser scanning microscope with 20× (NA 0.75), 40× (NA 1.30), and 63× (NA 1.40) oil-submersion objectives.

Neuronal reconstructions: CA1 pyramidal cells were reconstructed using Neurolucida 360 (ver. 2019.1.3; MBF Bioscience) as described previously (Shirinpour et al., 2021). Briefly, neuronal somata were reconstructed using the manual contour tracing option, with the contour tracing set to 'Cell Body'. Apical and basal dendrites as well as axons were subsequently reconstructed in the Neurolucida 3D environment under the 'User-guided' tracing option using the 'Directional Kernels' method.

Electric field modeling: Finite element method was used to create a three-dimensional mesh model consisting of two compartments, representing the bath solution and organotypic tissue cultures. The physical dimensions of the mesh model were based on the physical parameters of the in vitro settings, with a coil-to-Petri dish distance of 1 mm and the coil positioned above the culture. Electrical conductivities of 1.654 S/m and 0.275 S/m were assigned to the bath solution and culture respectively. The rate of change of the coil current was set to 1.4 A/ms at 1% MSO and scaled up to stimulation intensities ranging from 40 % to 60 % MSO. Simulations of macroscopic electric fields were performed using SimNIBS (3.2.6) and MATLAB (2023a). A validated 70 mm MagStim figure-of-eight coil was utilized in all simulations (Thielscher et al.,

bioRxiv preprint doi: https://doi.org/10.1101/2023.09.25.559399; this version posted September 27, 2023. The copyright holder for this preprint (which was not certified by peer review) is the author/funder. All rights reserved. No reuse allowed without permission.

2004). The 99th percentile of the E-field, which represents the robust maximum value, was extracted from the volume compartment of the tissue culture.

Single cell modelling: Reconstructions were imported into the NeMo-TMS pipeline and endowed with a Jarsky model (Jarsky et al., 2005). When axons are "swapped", the original axon is removed from the cell at the point of intersection with the soma or dendrite, and replaced with the axon of another cell that has been severed at the same point. Each cell is oriented with the apical dendrite pointing in the positive y direction, and axon orientations relative to this are preserved in the swapping process. For single-cell simulations, TMS is simulated as a uniform electric field of varying intensity, with the threshold defined as the smallest TMS amplitude that elicits a somatic action potential.

Experimental design and statistical analysis: Analyses were performed with the person analyzing the data blind to the experimental condition. For this project, we used one or two tissue cultures from each animal. Electrophysiological data were analyzed using pClamp 11.2 software suite (Molecular Devices), the Easy Electrophysiology 2.5.0.2 (Easy Electrophysiology Ltd.) and BrainWave (3Brain) software. Statistical comparisons were made using Mann–Whitney test (to compare two groups) two-way ANOVA and Kruskal-Wallis test as indicated in the figure captions and text (GraphPad Prism 7, GraphPad Software). p values of <0.05 were considered a significant difference. All values represent mean ± SEM.

Digital illustrations: Confocal image stacks were exported as 2D projections and stored as TIFF files. Figures were prepared using Photoshop graphics software (Adobe). Image brightness and contrast were adjusted.

bioRxiv preprint doi: https://doi.org/10.1101/2023.09.25.559399; this version posted September 27, 2023. The copyright holder for this preprint (which was not certified by peer review) is the author/funder. All rights reserved. No reuse allowed without permission.

RESULTS

10 Hz repetitive magnetic stimulation induces plasticity of excitatory and inhibitory synapses in mouse CA1 pyramidal neurons.

A 10 Hz stimulation protocol consisting of 900 pulses at 50% MSO was used to assess the effects of rMS on synaptic plasticity in brain tissue cultures prepared from mice of either sex (Fig. 1A-C). Individual CA1 pyramidal neurons were patched and AMPA receptor mediated mEPSCs were recorded 2 – 4 h after stimulation. In line with our previous work [c.f., (Vlachos et al., 2012; Lenz et al., 2015, 2020; Eichler et al., 2023)] a significant increase in mean mEPSC amplitude was observed as compared to age-/time-matched control cultures that were treated in the exact same way except for rMS (control; Figure 1D-E).

In a different set of cultures, we assessed 10 Hz rMS-induced changes in GABA receptor mediated mIPSCs onto CA1 pyramidal neurons using the experimental approach described above. A reduction in mean mIPSC amplitude was observed in these experiments as reported in our previous study [(Fig. 1F-G); c.f., (Lenz et al., 2016)]. These results confirm the robust effects of 10 Hz rMS on mEPSC and mIPSC amplitudes of CA1 pyramidal neurons of entorhino-hippocampal tissue cultures, which are consistent with a potentiation of excitatory synapses and a depression of inhibitory synapses.

10 Hz repetitive magnetic stimulation at 50% MSO does not affect synaptic strength in rat CA1 pyramidal neurons.

The effects of the same 10 Hz protocol (10 Hz, 900 pulses, 50% MSO) were tested in tissue cultures prepared from rat brains (Fig. 2). Age-matched rat tissue cultures displayed a larger cross-section than mouse tissue cultures (Fig. 2A), without any apparent morphological differences in

bioRxiv preprint doi: https://doi.org/10.1101/2023.09.25.559399; this version posted September 27, 2023. The copyright holder for this preprint (which was not certified by peer review) is the author/funder. All rights reserved. No reuse allowed without permission.

CA1 pyramidal neurons (Fig. 2B). Recordings of AMPA receptor mediated mEPSCs from CA1 pyramidal neurons showed no statically significant differences between control and 10 Hz rMS-stimulated preparations (Fig. 2A-B). Inhibitory synaptic strength was also unaffected, as no significant differences in mean mIPSC amplitude and frequency were detected 2 – 4 h after stimulation (Fig. 2C-D).

Macroscopic electric field simulations reveal distinct maximum electric fields generated in mouse and rat tissue cultures.

The electric field (E-field) strength induced in the mouse and rat slice cultures was described using computational modeling. Three-dimensional mesh models were created with two compartments (i.e., bath solution and slice cultures) using the finite element method (Fig. 3A). The physical dimensions of the mesh models were adapted from data obtain in mouse and rat brain issue cultures (Fig. 3B). Macroscopic modeling of the E-field revealed that stimulation at 50% MSO induces a stronger electric field in the mouse (20.4 V/m) when compared to the rat tissue culture (19.3 V/m). Based on the modeling we determined that 53 % MSO stimulation of rat tissue cultures would result in an E-field that is comparable to what we estimated in the mouse tissue cultures stimulated with 50 % MSO (Fig. 3C). Accordingly, another set of rat tissue cultures was stimulated with 53 % MSO (10 Hz, 900 pulses) and AMPA-receptor mediated mEPSCs were recorded from CA1 pyramidal neurons 2 – 4 h after stimulation. No significant differences in mean mEPSC amplitude and frequency were observed in these experiments (Fig. 3D). We conclude that simulation-based standardization of electric fields may not suffice to achieve comparable biological effects in mouse and rat CA1 pyramidal neurons, i.e., in neurons embedded in networks with comparable architectures and properties.

bioRxiv preprint doi: https://doi.org/10.1101/2023.09.25.559399; this version posted September 27, 2023. The copyright holder for this preprint (which was not certified by peer review) is the author/funder. All rights reserved. No reuse allowed without permission.

Baseline network activity is not significantly different between mouse and rat tissue cultures.

To test for differences in spontaneous network activity between mouse and rat entorhino-hippocampal slice cultures basal firing rates and field potential rates were recorded in a different set of 3-week-old mouse and rat tissue cultures using high-density microelectrode array recordings (Fig. 4A, B). No significant differences between mouse and rat tissue cultures were observed in firing and field potential (FP) rates in these experiments (Fig. 4C-F). We conclude that baseline network activity is not responsible for the inability of rMS to induce plasticity in rat CA1 pyramidal neurons.

No significant differences in structural properties of cultured mouse and rat CA1 pyramidal neurons.

To investigate whether differences in CA1 pyramidal neuron size and complexity could explain the variation in rMS outcome, we reconstructed biocytin-filled and streptavidin-A488 stained CA1 pyramidal neurons from both rat and mouse hippocampal tissue cultures and analyzed their dendrites and axons (Fig. 5). This was motivated by the observation that the brain sizes of mice and rats, as well as their tissue cultures, differ.

No significant differences were observed between the two groups in apical and basal dendritic length (Fig. 5C, D). Sholl and diameter/volume analyses (Fig. 5E-G) did not show any statistical significance between CA1 dendrites and their complexity of rat and mouse CA1 pyramidal neurons in entorhino-hippocampal tissue cultures. Similarly, no significant differences were observed when CA1 axons were reconstructed and compared in mouse and rat tissue cultures (Fig. 5I-L.) We conclude, that structural properties of individual CA1 pyramidal neurons are not

bioRxiv preprint doi: https://doi.org/10.1101/2023.09.25.559399; this version posted September 27, 2023. The copyright holder for this preprint (which was not certified by peer review) is the author/funder. All rights reserved. No reuse allowed without permission.

statistically different and cannot explain why the rat tissue cultures do not respond to 10 Hz rMS even when the E-field is closely matched based on e-field simulations.

Realistic multiscale computer modeling predicts no major differences in rMS-induced depolarization of mouse and rat CA1 pyramidal neurons

We assessed the impact of rMS on CA1 pyramidal neurons through a multiscale computational model that connects the physical input parameters of rMS to dendritic and axonal morphologies (Fig. 6). This approach was necessary because our morphological analysis might not have encompassed distinctions pertinent to the neuronal activation induced by rMS.

When examining the dendritic architecture of CA1 neurons in mice and rats, and employing a standardized artificial axon across all cells (c.f., Abbera et al., 2018; Shirinpour et al., 2021; Eichler et al., 2023), our simulations revealed no significant difference in the depolarization threshold elicited by rMS (Fig. 6A, B).

Subsequently, we investigated whether axonal morphologies might underlie the observed variability in our experimental outcomes. An additional series of simulations was conducted, this time integrating the authentic axonal morphologies of these neurons. Again, no significant differences in the depolarization thresholds were observed between the two groups (Fig. 6C).

A noteworthy insight emerged from these simulations: the axon's influence is pivotal in establishing the rMS-induced depolarization threshold (Table 1). We followed up on this observation, by establishing connections between the axons responsible for the lowest and highest rMS depolarization thresholds across all mouse and rat cells. Indeed, a 2-fold difference in the depolarization thresholds was observed in these simulations across all reconstructed neurons (Fig. 6D). Yet, despite these simulations results, the dissimilarity in rMS-triggered plasticity between

bioRxiv preprint doi: https://doi.org/10.1101/2023.09.25.559399; this version posted September 27, 2023. The copyright holder for this preprint (which was not certified by peer review) is the author/funder. All rights reserved. No reuse allowed without permission.

mouse and rat tissue cultures remained unresolved, eluding a complete explanation based solely on the interactions of dendritic and axonal morphologies.

Active and passive membrane properties reveal differences in excitability between mouse and rat CA1 pyramidal neurons

Next, active and passive membrane properties were recorded from CA1 pyramidal neurons and analyzed. Indeed, this set of experiments identified significant differences in the passive and active properties between mouse and rat CA1 pyramidal neurons (Fig. 7).

The input resistance of mouse CA1 pyramidal neurons was significantly higher as compared to rat CA1 pyramidal neurons (mouse: 156.8 ± 11.65 MOhm and rat: 67.25 ± 4.909 MOhm; Mann-Whitney test; $p < 0.001$; $U = 279$), while the cells of both mice and rats were resting at comparable membrane potentials (Fig. 7A-C). Consistently, the current-voltage (I/V) curves demonstrated that depolarizing mouse CA1 pyramidal neurons is more straightforward compared to cultured rat CA1 pyramidal neurons.

Looking at the active membrane properties (Fig. 7D-F) a similar trend was observed with the most striking differences being in the action potential induction threshold (mouse: -31.81 ± 0.877 mV; rat: -28.47 ± 0.744 mV; Mann-Whitney test; $p = 0.0021$; $U = 794$) and the first spike latency (mouse: 419.8 ± 56.03 ms; rat: 715 ± 77.36 ms; Mann-Whitney test; $p = 0.0074$; $U = 15$; data not shown). Figure 7F, shows that current injections produced stronger responses in mouse CA1 pyramidal neurons than in rat neurons, i.e., higher action potential frequencies at a lower current injection. These results indicated that mouse CA1 pyramidal neurons are more excitable than rat neurons, suggesting that higher stimulation intensities may be needed to induce rMS-induced plasticity in rat tissue cultures.

bioRxiv preprint doi: https://doi.org/10.1101/2023.09.25.559399; this version posted September 27, 2023. The copyright holder for this preprint (which was not certified by peer review) is the author/funder. All rights reserved. No reuse allowed without permission.

315 **60 % MSO induces rMS-mediated plasticity in rat organotypic tissue cultures**

316 Subsequently, we tested whether a 10 Hz stimulation protocol applied at a higher intensity would
317 induce plasticity in rat CA1 pyramidal neurons. Indeed, when rat tissue cultures were stimulated
318 with 10 Hz rMS at 60 % MSO a robust increase in the mean mEPSC amplitude was detected (Fig.
319 8A), similar to what we observe in the mouse cultures stimulated at 50 % MSO (cf. Fig. 1D and
320 Fig 3C). In addition, a significant reduction in mean mIPSC amplitude was evident 2 - 4 h after
321 rMS stimulation at 60 % MSO in a different set of rat tissue cultures (Fig. 8B; c.f., Fig. 1E). These
322 results demonstrate that rat CA1 pyramidal neurons do express rMS-induced plasticity, but require
323 a higher stimulation intensity for rMS-induced potentiation of excitatory synapses and depression
324 of inhibition to occur.

bioRxiv preprint doi: https://doi.org/10.1101/2023.09.25.559399; this version posted September 27, 2023. The copyright holder for this preprint (which was not certified by peer review) is the author/funder. All rights reserved. No reuse allowed without permission.

DISCUSSION

In this study, we investigated the cellular determinants governing the threshold for synaptic plasticity induced by 10 Hz rMS. To comprehensively examine the effects of neuronal structure, excitability, and network activity, we adopted a cross-species approach utilizing mouse and rat entorhino-hippocampal slice cultures. We confirmed the well-documented potentiation of excitatory synapses and depression of inhibitory synapses in mouse CA1 pyramidal neurons, reaffirming the robustness of rMS-induced synaptic plasticity under tightly controlled experimental conditions. However, despite comparable neuronal morphologies (both dendrites and axons) and no significant disparities in spontaneous network activity, the standardization of electric fields using prospective electric field modeling failed to yield the same biological effects in rat CA1 pyramidal neurons. Instead, we observed that adjusting the stimulation protocol to account for the distinct active and passive membrane properties, i.e., lower excitability of rat CA1 pyramidal neurons, led to both potentiation of excitatory synapses and depression of inhibitory synapses in rat CA1 pyramidal neurons. These findings highlight that the mere standardization of electric fields does not suffice to predict the after effects of rTMS even when neuronal morphologies and network activity are comparable. Accurate predictions require biophysically realistic compartmental models that reflect the intrinsic cellular properties of stimulated neurons and networks in distinct brain regions.

Over the past decade, the utilization of rTMS has experienced a significant surge in both research and clinical domains (Dayan et al., 2013; Paulus et al., 2013; Suppa et al., 2016; Blumberger et al., 2018; Lefaucheur et al., 2020; Lorentzen et al., 2022). Consequently, extensive efforts have been dedicated to identify the crucial parameters that influence the effects of rTMS on brain tissue (Deng et al., 2013; Lefaucheur et al., 2020; Zmeykina et al., 2020; Turi et al., 2021).

bioRxiv preprint doi: https://doi.org/10.1101/2023.09.25.559399; this version posted September 27, 2023. The copyright holder for this preprint (which was not certified by peer review) is the author/funder. All rights reserved. No reuse allowed without permission.

Among these parameters, the induced electric field emerges as a pivotal factor directly shaping the impact of rTMS on cortical tissue (Liu et al., 2018). While advancements in computational tools have enabled the calculation of rTMS-induced electric field (Thielscher et al., 2015), these models have primarily relied on mesoscopic structural parameters of the targeted stimulation area, i.e., head and brain geometries. In recent years, there has been a growing adoption of multi-scale modeling approaches to investigate the impact of TMS on individual neurons (Kamitani et al., 2001; Aberra et al., 2018, 2020; Shirinpour et al., 2021). Notably, these neuronal models are being integrated into mesoscopic brain models, enabling exploration of the effects of cortical folding and the precise positioning of neurons, such as distinguishing between the gyral crown and gyral groove, in individual subjects (Salvador et al., 2011; Seo and Jun, 2019; Aberra et al., 2020; Turi et al., 2022). While these models represent a significant advancement toward standardization and precision medicine in the field, it is increasingly evident that solely modeling electric fields and their interactions with individual neuronal morphologies (derived from animal models) may not be sufficient to standardize the biological effects of rTMS across various brain regions and individuals (Turi et al., 2022). The findings from this cross-species study present experimental evidence, underscoring the insufficiency of meticulous experimental standardization and electric field modeling in guaranteeing robust biological effects of rTMS. Notably, computational modeling revealed that rat slice cultures exhibited a weaker induced electric field, despite the size difference compared to mouse hippocampal tissue cultures. However, even when efforts were made to match the generated electric fields between mouse and rat tissue cultures, it proved inadequate in reproducing the desired plasticity effects in the rat tissue cultures.

In this context, it is crucial to highlight that our experiments revealed no statistically significant morphological differences between the cultured CA1 pyramidal neurons of mice and

bioRxiv preprint doi: https://doi.org/10.1101/2023.09.25.559399; this version posted September 27, 2023. The copyright holder for this preprint (which was not certified by peer review) is the author/funder. All rights reserved. No reuse allowed without permission.

rats. The comprehensive analysis of both apical and basal dendrites demonstrated comparable total dendritic length, complexity, and overall volume in both rat and mouse pyramidal neurons of organotypic tissue cultures. These results align with previously published data that compared mouse and rat hippocampal CA1 neurons in acute slice preparations (Routh et al., 2009). However, it is worth noting that the total volume of these cells, apart from the observed morphologies features, was found to be higher in rat slices. While we cannot completely dismiss the possibility that the observed discrepancy may be attributed to differences between acute brain slices and tissue culture slices, it is essential to highlight a major advantage of tissue cultures. Specifically, the inclusion of 3-week-old tissue cultures, allowed for the assessment of neurons that are not acutely lesioned or denervation due to prior acute slicing, offering a distinct advantage in our study. This enabled us to study CA1 pyramidal neurons under steady state conditions and to reconstruct complete neuronal morphologies, encompassing the entire dendritic tree and axonal compartment. Such comprehensive reconstructions are deemed critical for accurately assessing the outcomes rTMS, as the interaction between the generated electric field and axons is of paramount importance (Siebner et al., 2022). Importantly, our investigation revealed no significant disparities in the axonal properties of cultured CA1 neurons between mice and rats. This finding suggests that the observed inability of rat CA1 neurons to exhibit synaptic plasticity cannot be trivially attributed to differences in axonal characteristics.

Nevertheless, our simulations provided robust experimental evidence that axon morphology matters. We identified axons that, upon exposure to electromagnetic fields, proved twice as effective at depolarizing neurons compared to their counterparts—this efficacy transcending the attached somata and dendritic morphologies. These insights call for a methodical evaluation of diverse axonal morphologies concerning rTMS-induced synaptic plasticity. These

bioRxiv preprint doi: https://doi.org/10.1101/2023.09.25.559399; this version posted September 27, 2023. The copyright holder for this preprint (which was not certified by peer review) is the author/funder. All rights reserved. No reuse allowed without permission.

394 inquiries should encompass considerations of myelination levels and the potential influence of
395 oligodendrocytes on the depolarization and induction of plasticity prompted by rTMS. It is our
396 proposition that within complex cortical networks, the existence of "super-responder cells" might
397 be plausible—entities uniquely attuned to rTMS at a given stimulation intensity. This notion finds
398 support in the observation that not all neurons of this and our previous studies (c.f., Vlachos et al.,
399 2012; Lenz et al., 2016; Lenz et al., 2020; Eichler et al., 2023) displayed elevated mEPSC
400 amplitudes or decreased mIPSC within the 2 – 4 h following stimulation. Consequently,
401 uncovering the mechanistic basis of this variability becomes paramount, as it could illuminate the
402 neural substrates and signaling pathways underlying the multifaceted response patterns induced
403 by rTMS.

404 The results of the present study suggest that understanding the differential effects of rTMS
405 in mouse and rat CA1 pyramidal neurons necessitates the consideration of intrinsic cellular
406 properties. Neglecting these properties impedes our comprehensive explanation and prediction of
407 observed differences in plasticity induction thresholds. In line with previous research on acute rat
408 and mouse slices (Routh et al., 2009), our study revealed that rat CA1 pyramidal neurons exhibit
409 a more depolarized action potential threshold compared to mice. This distinction renders rat
410 neurons comparatively more resistant to excitation. Interestingly, our findings provide additional
411 evidence by demonstrating that rat CA1 neurons possess significantly lower input resistance
412 relative to their mouse counterparts. This observation reinforces the concept of reduced excitability
413 in rat neurons. It is important to note, however, that the study by Routh and colleagues (2009)
414 reported comparable input resistance between the two species, potentially attributable to the impact
415 of acute slicing on neuronal integrity as discussed above.

bioRxiv preprint doi: https://doi.org/10.1101/2023.09.25.559399; this version posted September 27, 2023. The copyright holder for this preprint (which was not certified by peer review) is the author/funder. All rights reserved. No reuse allowed without permission.

Can morphological and biophysical properties alone provide sufficient prediction of biologically relevant outcomes of rTMS? It is clear that additional factors can affect cortical excitability, subsequently influencing how neurons respond to rTMS and modifying both the threshold, magnitude, and direction of rTMS-induced plasticity. Neuromodulators, such as dopamine, serotonin and noradrenaline have been demonstrated to regulate cortical excitability in both healthy and pathological conditions (Greenberg et al., 2000; Nitsche et al., 2006; Martorana et al., 2009; Michael A Nitsche et al., 2010; le Grand et al., 2011; Kuo et al., 2017). Specifically, dopamine has been implicated in the modulation of cortical excitability during action observation with TMS in human subjects (Strafella and Paus, 2000). Furthermore, neuromodulators can impact the capacity of neurons to express plasticity without affecting excitability and other baseline functional and structural properties of neurons and neural networks, a phenomenon known as metaplasticity (Abraham and Bear, 1996; Seol et al., 2007). It is important to also note that non-neuronal cells can significantly influence the capacity of neurons to express synaptic plasticity (Stellwagen et al., 2005; Henneberger et al., 2010; Allen, 2014; Andoh and Koyama, 2021; Sancho et al., 2021; Kleidonas et al., 2023). Our prior work has provided evidence that cytokines derived from microglia play a crucial role in facilitating rTMS-induced plasticity (Eichler et al., 2023). Finally, the impact of network activity on plasticity thresholds and the outcome or rTMS must be considered. These factors collectively underscore the multifaceted nature of the processes involved in influencing and modulating the outcomes of rTMS-induced plasticity. Organotypic slice cultures serve as valuable tools for investigating these and other aspects of rTMS-induced plasticity, highlighting the necessity for rigorously validated computer models that link the induced electric fields with biophysically realistic neurons and networks. These models hold the potential to predict the biological outcomes of rTMS, offering valuable insights into its effects and guiding

bioRxiv preprint doi: https://doi.org/10.1101/2023.09.25.559399; this version posted September 27, 2023. The copyright holder for this preprint (which was not certified by peer review) is the author/funder. All rights reserved. No reuse allowed without permission.

439 the adaptation of stimulation protocols to achieve consisted desired effects across different brain

440 regions and individuals.

bioRxiv preprint doi: https://doi.org/10.1101/2023.09.25.559399; this version posted September 27, 2023. The copyright holder for this preprint (which was not certified by peer review) is the author/funder. All rights reserved. No reuse allowed without permission.

REFERENCES

Aberra AS, Peterchev AV, Grill WM (2018) Biophysically realistic neuron models for simulation of cortical stimulation. J Neural Eng 15:066023.

Aberra AS, Wang B, Grill WM, Peterchev AV (2020) Simulation of transcranial magnetic stimulation in head model with morphologically-realistic cortical neurons. Brain Stimul 13:175–189.

Abraham WC, Bear MF (1996) Metaplasticity: the plasticity of synaptic plasticity. Trends Neurosci 19:126–130.

Allen NJ (2014) Astrocyte regulation of synaptic behavior. Annu Rev Cell Dev Biol 30:439–463.

Andoh M, Koyama R (2021) Microglia regulate synaptic development and plasticity. Dev Neurobiol 81:568–590.

Blumberger DM, Vila-Rodriguez F, Thorpe KE, Feffer K, Noda Y, Giacobbe P, Knyahnytska Y, Kennedy SH, Lam RW, Daskalakis ZJ, Downar J (2018) Effectiveness of theta burst versus high-frequency repetitive transcranial magnetic stimulation in patients with depression (THREE-D): a randomised non-inferiority trial. Lancet 391:1683–1692.

Chen R, Classen J, Gerloff C, Celnik P, Wassermann EM, Hallett M, Cohen LG (1997) Depression of motor cortex excitability by low-frequency transcranial magnetic stimulation. Neurology 48:1398–1403.

Cirillo G, Di Pino G, Capone F, Ranieri F, Florio L, Todisco V, Tedeschi G, Funke K, Di Lazzaro V (2017) Neurobiological after-effects of non-invasive brain stimulation. Brain Stimul 10:1–18.

Cocchi L, Zalesky A, Nott Z, Whybird G, Fitzgerald PB, Breakspear M (2018) Transcranial magnetic stimulation in obsessive-compulsive disorder: A focus on network mechanisms and state dependence. Neuroimage Clin 19:661–674.

Dayan E, Censor N, Buch ER, Sandrini M, Cohen LG (2013) Noninvasive brain stimulation: from physiology to network dynamics and back. Nat Neurosci 16:838–844.

Deng Z-D, Lisanby SH, Peterchev AV (2013) Electric field depth-focality tradeoff in transcranial magnetic stimulation: simulation comparison of 50 coil designs. Brain Stimul 6:1–13.

Eichler A, Kleidonas D, Turi Z, Fliegauf M, Kirsch M, Pfeifer D, Masuda T, Prinz M, Lenz M, Vlachos A (2023) Microglial Cytokines Mediate Plasticity Induced by 10 Hz Repetitive Magnetic Stimulation. J Neurosci 43:3042–3060.

Garnaat SL, Yuan S, Wang H, Philip NS, Carpenter LL (2018) Updates on Transcranial Magnetic Stimulation Therapy for Major Depressive Disorder. Psychiatr Clin North Am 41:419–431.

Goldsworthy MR, Müller-Dahlhaus F, Ridding MC, Ziemann U (2014) Inter-subject variability of LTD-like plasticity in human motor cortex: a matter of preceding motor activation. Brain Stimul 7:864–870.

Greenberg BD, Ziemann U, Corá-Locatelli G, Harmon A, Murphy DL, Keel JC, Wassermann EM (2000) Altered cortical excitability in obsessive–compulsive disorder. Neurology 54:142–142.

bioRxiv preprint doi: https://doi.org/10.1101/2023.09.25.559399; this version posted September 27, 2023. The copyright holder for this preprint (which was not certified by peer review) is the author/funder. All rights reserved. No reuse allowed without permission.

Guerra A, López-Alonso V, Cheeran B, Suppa A (2020) Variability in non-invasive brain stimulation studies: Reasons and results. Neuroscience Letters 719:133330.

Henneberger C, Papouin T, Oliet SHR, Rusakov DA (2010) Long-term potentiation depends on release of D-serine from astrocytes. Nature 463:232–236.

Hong Y, Liu Q, Peng M, Bai M, Li J, Sun R, Guo H, Xu P, Xie Y, Li Y, Liu L, Du J, Liu X, Yang B, Xu G (2020) High-frequency repetitive transcranial magnetic stimulation improves functional recovery by inhibiting neurotoxic polarization of astrocytes in ischemic rats. J Neuroinflammation 17:150.

Huang Y-Z, Edwards MJ, Rounis E, Bhatia KP, Rothwell JC (2005) Theta Burst Stimulation of the Human Motor Cortex. Neuron 45:201–206.

Jarsky T, Roxin A, Kath WL, Spruston N (2005) Conditional dendritic spike propagation following distal synaptic activation of hippocampal CA1 pyramidal neurons. Nat Neurosci 8:1667–1676.

Kamitani Y, Bhalodia VM, Kubota Y, Shimojo S (2001) A model of magnetic stimulation of neocortical neurons. Neurocomputing 38–40:697–703.

Kleidonas D, Kirsch M, Andrieux G, Pfeifer D, Boerries M, Vlachos A (2023) Microglia modulate TNFα-mediated synaptic plasticity. Glia 71:2117–2136.

Kuo H-I, Paulus W, Batsikadze G, Jamil A, Kuo M-F, Nitsche MA (2017) Acute and Chronic Noradrenergic Effects on Cortical Excitability in Healthy Humans. Int J Neuropsychopharmacol 20:634–643.

le Grand SM, Supornsilpchai W, Saengjaroentham C, Srikiatkhachorn A (2011) Serotonin Depletion Leads to Cortical Hyperexcitability and Trigeminal Nociceptive Facilitation via the Nitric Oxide Pathway. Headache: The Journal of Head and Face Pain 51:1152–1160.

Lefaucheur J-P et al. (2020) Evidence-based guidelines on the therapeutic use of repetitive transcranial magnetic stimulation (rTMS): An update (2014-2018). Clin Neurophysiol 131:474–528.

Lenz M, Eichler A, Kruse P, Strehl A, Rodriguez-Rozada S, Goren I, Yogev N, Frank S, Waisman A, Deller T, Jung S, Maggio N, Vlachos A (2020) Interleukin 10 Restores Lipopolysaccharide-Induced Alterations in Synaptic Plasticity Probed by Repetitive Magnetic Stimulation. Front Immunol 11:614509.

Lenz M, Galanis C, Müller-Dahlhaus F, Opitz A, Wierenga CJ, Szabó G, Ziemann U, Deller T, Funke K, Vlachos A (2016) Repetitive magnetic stimulation induces plasticity of inhibitory synapses. Nat Commun 7:10020.

Lenz M, Platschek S, Priesemann V, Becker D, Willems LM, Ziemann U, Deller T, Müller-Dahlhaus F, Jedlicka P, Vlachos A (2015) Repetitive magnetic stimulation induces plasticity of excitatory postsynapses on proximal dendrites of cultured mouse CA1 pyramidal neurons. Brain Struct Funct 220:3323–3337.

Liu A, Vöröslakos M, Kronberg G, Henin S, Krause MR, Huang Y, Opitz A, Mehta A, Pack CC, Krekelberg B, Berényi A, Parra LC, Melloni L, Devinsky O, Buzsáki G (2018) Immediate neurophysiological effects of transcranial electrical stimulation. Nat Commun 9:5092.

López-Alonso V, Cheeran B, Río-Rodríguez D, Fernández-Del-Olmo M (2014) Inter-individual variability in response to non-invasive brain stimulation paradigms. Brain Stimul 7:372–380.

bioRxiv preprint doi: https://doi.org/10.1101/2023.09.25.559399; this version posted September 27, 2023. The copyright holder for this preprint (which was not certified by peer review) is the author/funder. All rights reserved. No reuse allowed without permission.

Lorentzen R, Nguyen TD, McGirr A, Hieronymus F, Østergaard SD (2022) The efficacy of transcranial magnetic stimulation (TMS) for negative symptoms in schizophrenia: a systematic review and meta-analysis. Schizophr 8:1–12.

Martorana A, Mori F, Esposito Z, Kusayanagi H, Monteleone F, Codecà C, Sancesario G, Bernardi G, Koch G (2009) Dopamine Modulates Cholinergic Cortical Excitability in Alzheimer's Disease Patients. Neuropsychopharmacol 34:2323–2328.

Michael A Nitsche, Katia Monte-Silva, Min-Fang Kuo, Walter Paulus (2010) Dopaminergic Impact on Cortical Excitability in Humans. Reviews in the Neurosciences 21:289–298.

Moretti J, Terstege DJ, Poh EZ, Epp JR, Rodger J (2022) Low intensity repetitive transcranial magnetic stimulation modulates brain-wide functional connectivity to promote anti-correlated c-Fos expression. Sci Rep 12:20571.

Müller-Dahlhaus F, Vlachos A (2013) Unraveling the cellular and molecular mechanisms of repetitive magnetic stimulation. Front Mol Neurosci 6:50.

Nitsche MA, Lampe C, Antal A, Liebetanz D, Lang N, Tergau F, Paulus W (2006) Dopaminergic modulation of long-lasting direct current-induced cortical excitability changes in the human motor cortex. European Journal of Neuroscience 23:1651–1657.

Opitz A, Windhoff M, Heidemann RM, Turner R, Thielscher A (2011) How the brain tissue shapes the electric field induced by transcranial magnetic stimulation. Neuroimage 58:849–859.

Paulus W, Peterchev AV, Ridding M (2013) Transcranial electric and magnetic stimulation: technique and paradigms. Handb Clin Neurol 116:329–342.

Peterchev AV, Wagner TA, Miranda PC, Nitsche MA, Paulus W, Lisanby SH, Pascual-Leone A, Bikson M (2012) Fundamentals of transcranial electric and magnetic stimulation dose: definition, selection, and reporting practices. Brain Stimul 5:435–453.

Rehn S, Eslick GD, Brakoulias V (2018) A Meta-Analysis of the Effectiveness of Different Cortical Targets Used in Repetitive Transcranial Magnetic Stimulation (rTMS) for the Treatment of Obsessive-Compulsive Disorder (OCD). Psychiatr Q 89:645–665.

Romero MC, Merken L, Janssen P, Davare M (2022) Neural effects of continuous theta-burst stimulation in macaque parietal neurons. Elife 11:e65536.

Routh BN, Johnston D, Harris K, Chitwood RA (2009) Anatomical and Electrophysiological Comparison of CA1 Pyramidal Neurons of the Rat and Mouse. J Neurophysiol 102:2288–2302.

Salvador R, Silva S, Basser PJ, Miranda PC (2011) Determining which mechanisms lead to activation in the motor cortex: a modeling study of transcranial magnetic stimulation using realistic stimulus waveforms and sulcal geometry. Clin Neurophysiol 122:748–758.

Sancho L, Contreras M, Allen NJ (2021) Glia as sculptors of synaptic plasticity. Neurosci Res 167:17–29.

Saturnino GB, Puonti O, Nielsen JD, Antonenko D, Madsen KH, Thielscher A (2019) SimNIBS 2.1: A Comprehensive Pipeline for Individualized Electric Field Modelling for Transcranial Brain Stimulation. In: Brain and Human Body Modeling: Computational Human Modeling at EMBC 2018 (Makarov S, Horner

bioRxiv preprint doi: https://doi.org/10.1101/2023.09.25.559399; this version posted September 27, 2023. The copyright holder for this preprint (which was not certified by peer review) is the author/funder. All rights reserved. No reuse allowed without permission.

M, Noetscher G, eds). Cham (CH): Springer. Available at: http://www.ncbi.nlm.nih.gov/books/NBK549569/ [Accessed June 13, 2023].

Seo H, Jun SC (2019) Relation between the electric field and activation of cortical neurons in transcranial electrical stimulation. Brain Stimulation 12:275–289.

Seol GH, Ziburkus J, Huang S, Song L, Kim IT, Takamiya K, Huganir RL, Lee H-K, Kirkwood A (2007) Neuromodulators Control the Polarity of Spike-Timing-Dependent Synaptic Plasticity. Neuron 55:919–929.

Shirinpour S, Hananeia N, Rosado J, Tran H, Galanis C, Vlachos A, Jedlicka P, Queisser G, Opitz A (2021) Multi-scale modeling toolbox for single neuron and subcellular activity under Transcranial Magnetic Stimulation. Brain Stimul 14:1470–1482.

Siebner HR et al. (2022) Transcranial magnetic stimulation of the brain: What is stimulated? – A consensus and critical position paper. Clin Neurophysiol 140:59–97.

Somaa FA, de Graaf TA, Sack AT (2022) Transcranial Magnetic Stimulation in the Treatment of Neurological Diseases. Front Neurol 13:793253.

Stellwagen D, Beattie EC, Seo JY, Malenka RC (2005) Differential regulation of AMPA receptor and GABA receptor trafficking by tumor necrosis factor-alpha. J Neurosci 25:3219–3228.

Strafella AP, Paus T (2000) Modulation of cortical excitability during action observation: a transcranial magnetic stimulation study. Neuroreport 11:2289–2292.

Suppa A, Huang Y-Z, Funke K, Ridding MC, Cheeran B, Di Lazzaro V, Ziemann U, Rothwell JC (2016) Ten Years of Theta Burst Stimulation in Humans: Established Knowledge, Unknowns and Prospects. Brain Stimulation 9:323–335.

Tang AD, Bennett W, Bindoff AD, Bolland S, Collins J, Langley RC, Garry MI, Summers JJ, Hinder MR, Rodger J, Canty AJ (2021) Subthreshold repetitive transcranial magnetic stimulation drives structural synaptic plasticity in the young and aged motor cortex. Brain Stimulation 14:1498–1507.

Thielscher A, Antunes A, Saturnino GB (2015) Field modeling for transcranial magnetic stimulation: A useful tool to understand the physiological effects of TMS? In: 2015 37th Annual International Conference of the IEEE Engineering in Medicine and Biology Society (EMBC), pp 222–225.

Thielscher A, Opitz A, Windhoff M (2011) Impact of the gyral geometry on the electric field induced by transcranial magnetic stimulation. Neuroimage 54:234–243.

Tokay T, Holl N, Kirschstein T, Zschorlich V, Köhling R (2009) High-frequency magnetic stimulation induces long-term potentiation in rat hippocampal slices. Neurosci Lett 461:150–154.

Tokay T, Kirschstein T, Rohde M, Zschorlich V, Köhling R (2014) NMDA receptor-dependent metaplasticity by high-frequency magnetic stimulation. Neural Plast 2014:684238.

Turi Z, Hananeia N, Shirinpour S, Opitz A, Jedlicka P, Vlachos A (2022) Dosing Transcranial Magnetic Stimulation of the Primary Motor and Dorsolateral Prefrontal Cortices With Multi-Scale Modeling. Front Neurosci 16:929814.

bioRxiv preprint doi: https://doi.org/10.1101/2023.09.25.559399; this version posted September 27, 2023. The copyright holder for this preprint (which was not certified by peer review) is the author/funder. All rights reserved. No reuse allowed without permission.

585 Turi Z, Lenz M, Paulus W, Mittner M, Vlachos A (2021) Selecting stimulation intensity in repetitive
586 transcranial magnetic stimulation studies: A systematic review between 1991 and 2020. European
587 Journal of Neuroscience 53:3404–3415.

588 Vallence A-M, Goldsworthy MR, Hodyl NA, Semmler JG, Pitcher JB, Ridding MC (2015) Inter- and intra-
589 subject variability of motor cortex plasticity following continuous theta-burst stimulation. Neuroscience
590 304:266–278.

591 Vlachos A, Müller-Dahlhaus F, Rosskopp J, Lenz M, Ziemann U, Deller T (2012) Repetitive magnetic
592 stimulation induces functional and structural plasticity of excitatory postsynapses in mouse organotypic
593 hippocampal slice cultures. J Neurosci 32:17514–17523.

594 Voigt J, Carpenter L, Leuchter A (2019) A systematic literature review of the clinical efficacy of repetitive
595 transcranial magnetic stimulation (rTMS) in non-treatment resistant patients with major depressive
596 disorder. BMC Psychiatry 19:13.

597 Zmeykina E, Mittner M, Paulus W, Turi Z (2020) Weak rTMS-induced electric fields produce neural
598 entrainment in humans. Sci Rep 10:11994.

bioRxiv preprint doi: https://doi.org/10.1101/2023.09.25.559399; this version posted September 27, 2023. The copyright holder for this preprint (which was not certified by peer review) is the author/funder. All rights reserved. No reuse allowed without permission.

FIGURE LEGENDS

Figure 1: 10 Hz repetitive magnetic stimulation (rMS) at 50% MSO induces synaptic plasticity in mouse CA1 pyramidal neurons.

(A) Schematic illustration of the experimental setting. Organotypic tissue cultures are stimulated in a standard 35 mm petri dish filled with extracellular solution using a 70 mm figure-of-eight coil (900 pulses, 10 Hz, at 50 % maximum stimulator output). **(B)** Overview of an organotypic tissue culture. DAPI nuclear staining was used for visualization of cytoarchitecture. DG, Dentate gyrus; EC, entorhinal cortex; CA1 and CA3, *Cornu Ammonis* areas 1 and 3. Scale bar, 500 µm. **(C)** Patched CA1 pyramidal neurons filled with biocytin and identified *post hoc* with streptavidin-A488. Scale bar, 50 µm. **(D, E)** Sample traces and group data of AMPA receptor mediated miniature excitatory post synaptic currents (mEPSCs) recorded from mouse CA1 pyramidal neurons in sham-(control) and rMS-stimulated cultures 2 – 4 h after stimulation (control, n = 31 cells; rMS, n = 28 cells; Mann–Whitney test). **(F, G)** Sample traces and group data of GABA receptor mediated miniature inhibitory post synaptic currents (mIPSCs) recorded from mouse CA1 pyramidal neurons in sham-(control) and rMS-stimulated cultures 2 – 4 h after stimulation (control, n = 14 cells; rMS, n = 14 cells; Mann–Whitney test). Individual data points are indicated in this and the following figures by gray dots. Data are mean ± SEM. NS, Not significant. *$p < 0.05$. **$p < 0.01$.

Figure 2: 10 Hz repetitive magnetic stimulation (rMS) at 50 % maximum stimulator output does not affect synaptic transmission in rat CA1 pyramidal neurons.

(A) Overview images of a mouse and rat organotypic tissue culture. DG, Dentate gyrus; EC, entorhinal cortex; CA1 and CA3, *Cornu Ammonis* areas 1 and 3. Scale bar, 500 µm. **(C)** Patched rat CA1 pyramidal neurons filled with biocytin and identified *post hoc* with streptavidin-A488.

bioRxiv preprint doi: https://doi.org/10.1101/2023.09.25.559399; this version posted September 27, 2023. The copyright holder for this preprint (which was not certified by peer review) is the author/funder. All rights reserved. No reuse allowed without permission.

Scale bar, 50 µm. **(C, D)** Sample traces and group data of AMPA receptor mediated mEPSCs recorded from rat CA1 pyramidal neurons in sham-(control) and rMS-stimulated cultures 2 – 4 h after stimulation (control, n = 38 cells; rMS, n = 71 cells; Mann–Whitney test). **(E, F)** Sample traces and group data of GABA receptor mediated miniature inhibitory post synaptic currents (mIPSCs) recorded from rat CA1 pyramidal neurons in sham-(control) and rMS-stimulated cultures 2 – 4 h after stimulation (control, n = 12 cells; rMS, n = 9 cells; Mann–Whitney test). Data are mean ± SEM. NS, Not significant.

Figure 3: Modeling of repetitive magnetic stimulation (rMS)-induced electric fields in mouse and rat tissue cultures.

(A) Visualization of the macroscopic electric field simulations generated by rMS *in vitro*. **(B)** Three-dimensional mesh models of mouse and rat organotypic tissue cultures and the electric fields generated by a single-pulse of rMS, respectively. **(C)** Comparison of the maximum electric field generated at distinct stimulation intensities in mouse and rat tissue cultures. The electric field generated in mouse slice cultures at 50 % maximum stimulator output is attained with 53% maximum stimulator output in rat tissue cultures. **(D)** Group data of AMPA receptor mediated mEPSCs recorded from rat CA1 pyramidal neurons in sham-(control) and rMS-stimulated cultures stimulated with 53 % maximum stimulator output and recorded 2 – 4 h after stimulation (control, n = 12 cells; rMS, n = 12 cells; Mann–Whitney test). Data are mean ± SEM. NS, Not significant.

Figure 4: No significant differences in baseline network activity in mouse and rat tissue cultures.

bioRxiv preprint doi: https://doi.org/10.1101/2023.09.25.559399; this version posted September 27, 2023. The copyright holder for this preprint (which was not certified by peer review) is the author/funder. All rights reserved. No reuse allowed without permission.

642 **(A-B)** Overview images of mouse and rat tissue culture on high-density multi electrode array chips.
643 DG, Dentate gyrus; EC, entorhinal cortex; CA1 and CA3, *Cornu Ammonis* areas 1 and 3. **(C)**
644 Raster plots of spikes during a 10-minute recording period in whole mouse and rat tissue cultures.
645 **(D-F)** Group data of mean firing rate and mean field potential rate from mouse and rat tissue
646 cultures (mouse, n = 4 cultures; rat, n = 5 cultures; Mann–Whitney test). Data are mean ± SEM.
647 NS, Not significant.

648 **Figure 5: No significant morphological differences of CA1 pyramidal neurons in mouse and**
649 **rat tissue cultures.**
650 **(A, B**) Examples of CA1 pyramidal neurons that were patched and filled with biocytin, later
651 identified *post hoc* with streptavidin-A488, along with three-dimensional neuronal reconstructions
652 of both mouse and rat CA1 pyramidal neurons. **(C-H)** Group data of mouse and rat apical and
653 basal dendrites (mouse, n = 11 cells; rat, n = 11 cells; statistical comparisons for panels C, D, G
654 and H were performed with Mann–Whitney test; statistical comparisons for panels E and F were
655 performed with 2-way ANOVA). **(I)** Rat CA1 pyramidal neuron patched and filled with biocytin,
656 identified *post hoc* with streptavidin-A488, and used for comprehensive neuronal reconstruction,
657 encompassing dendritic and axonal neuronal structures. Scale bar, 50 µm. **(J-L)** Group data of
658 mouse and rat axons (mouse, n = 6 cells; rat, n = 6 cells; statistical comparisons for panels J and L
659 were performed with Mann–Whitney test; statistical comparisons for panel K were performed with
660 2-way ANOVA).

661 **Figure 6: Multiscale computer modeling of electromagnetic stimulation.**

bioRxiv preprint doi: https://doi.org/10.1101/2023.09.25.559399; this version posted September 27, 2023. The copyright holder for this preprint (which was not certified by peer review) is the author/funder. All rights reserved. No reuse allowed without permission.

(A) Neuronal responses, i.e., changes in membrane voltage, to electromagnetic stimulation were modeled in realistic dendritic and axonal morphologies from reconstructed mouse and rat CA1 pyramidal neurons. (B) Group data of realistic dendritic morphologies with a standardized artificial axon (mouse, n = 6 cells; rat, n = 6 cells; Mann–Whitney test). (C) Group data of simulations with realistic dendritic and axonal morphologies (mouse, n = 6 cells; rat, n = 6 cells; Mann–Whitney test). (D) Group data for mouse and rat CA1 pyramidal neurons, categorizing those with axons exhibiting lowest (left) and highest (right) rMS depolarization thresholds (mouse, n = 6 cells; rat, n = 6 cells; Kruskal-Wallis test). Data are mean ± SEM. NS, Not significant.

Figure 7: Rat CA1 pyramidal neurons exhibit lower excitability in comparison to mice.

(A) Sample traces from input-output recordings of CA1 pyramidal neurons of mouse and rat tissue cultures. **(B, C)** Group data of resting membrane potential and input resistance from mouse and rat CA1 pyramidal neurons (mouse, n = 44 cells; rat, n = 56 cells; Mann–Whitney test). **(D, E)** Group data of action potential (AP) amplitude and threshold from mouse and rat CA1 pyramidal neurons (mouse, n = 44 cells; rat, n = 56 cells; Mann–Whitney test). **(F)** I-F curve of CA1 pyramidal neurons of mouse and rat tissue cultures (mouse, n = 52 cells; rat, n = 63 cells; 2-way ANOVA). Data are mean ± SEM. NS, Not significant. **p < 0.01. ***p < 0.001.

Figure 8: 10 Hz repetitive magnetic stimulation (rMS) at 60 % MSO induces synaptic plasticity in rat CA1 pyramidal neurons.

(A) Group data of AMPA receptor mediated mEPSCs recorded from rat CA1 pyramidal neurons from sham- (control) and rMS- stimulated cultures (control, n = 34 cells; rMS, n = 16 cells; Mann–Whitney test). (C, D) Sample traces and group data of miniature

bioRxiv preprint doi: https://doi.org/10.1101/2023.09.25.559399; this version posted September 27, 2023. The copyright holder for this preprint (which was not certified by peer review) is the author/funder. All rights reserved. No reuse allowed without permission.

683 inhibitory post synaptic currents (mIPSCs) recorded from rat CA1 pyramidal neurons from
684 sham- (control) and rMS- stimulated cultures (control, $n = 14$ cells; rMS, $n = 17$ cells;
685 Mann–Whitney test. One data point outside of axis limits in mIPSC amplitude and
686 frequency respectively). Data are mean ± SEM. NS, Not significant. $*p < 0.05$.
687 $***p < 0.001$.

bioRxiv preprint doi: https://doi.org/10.1101/2023.09.25.559399; this version posted September 27, 2023. The copyright holder for this preprint (which was not certified by peer review) is the author/funder. All rights reserved. No reuse allowed without permission.

Figure 1

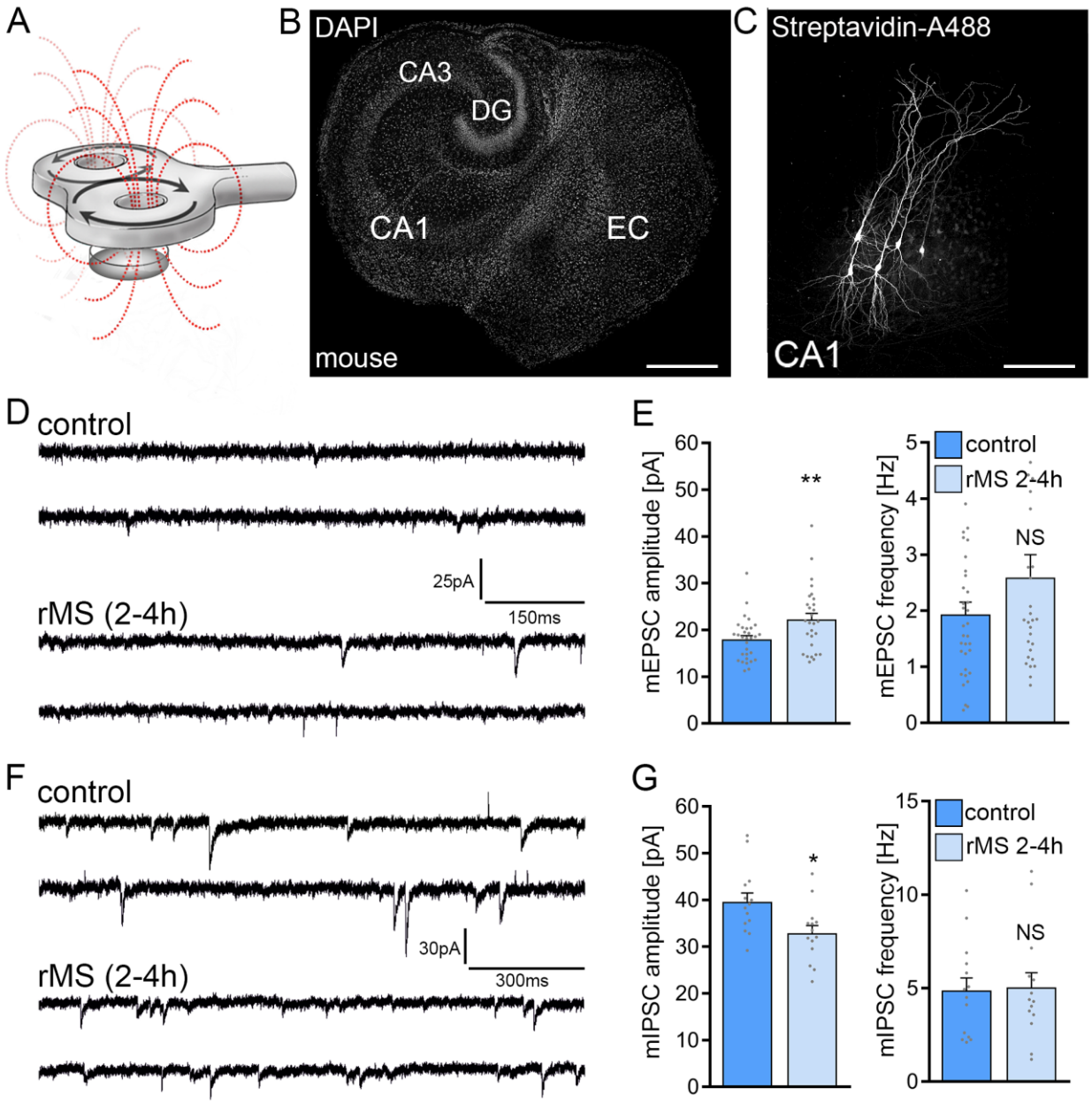

bioRxiv preprint doi: https://doi.org/10.1101/2023.09.25.559399; this version posted September 27, 2023. The copyright holder for this preprint (which was not certified by peer review) is the author/funder. All rights reserved. No reuse allowed without permission.

Figure 2

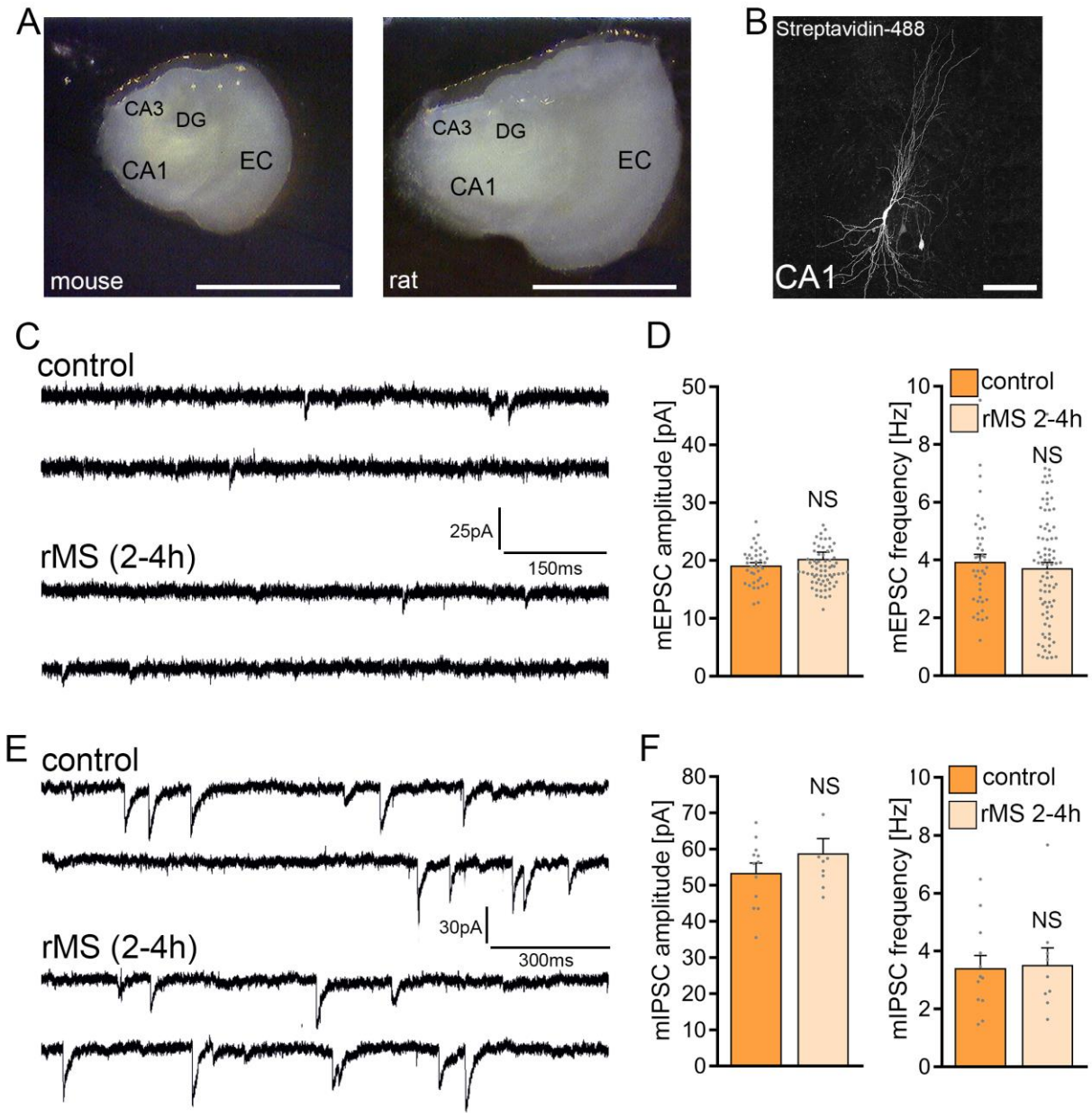

bioRxiv preprint doi: https://doi.org/10.1101/2023.09.25.559399; this version posted September 27, 2023. The copyright holder for this preprint (which was not certified by peer review) is the author/funder. All rights reserved. No reuse allowed without permission.

Figure 3

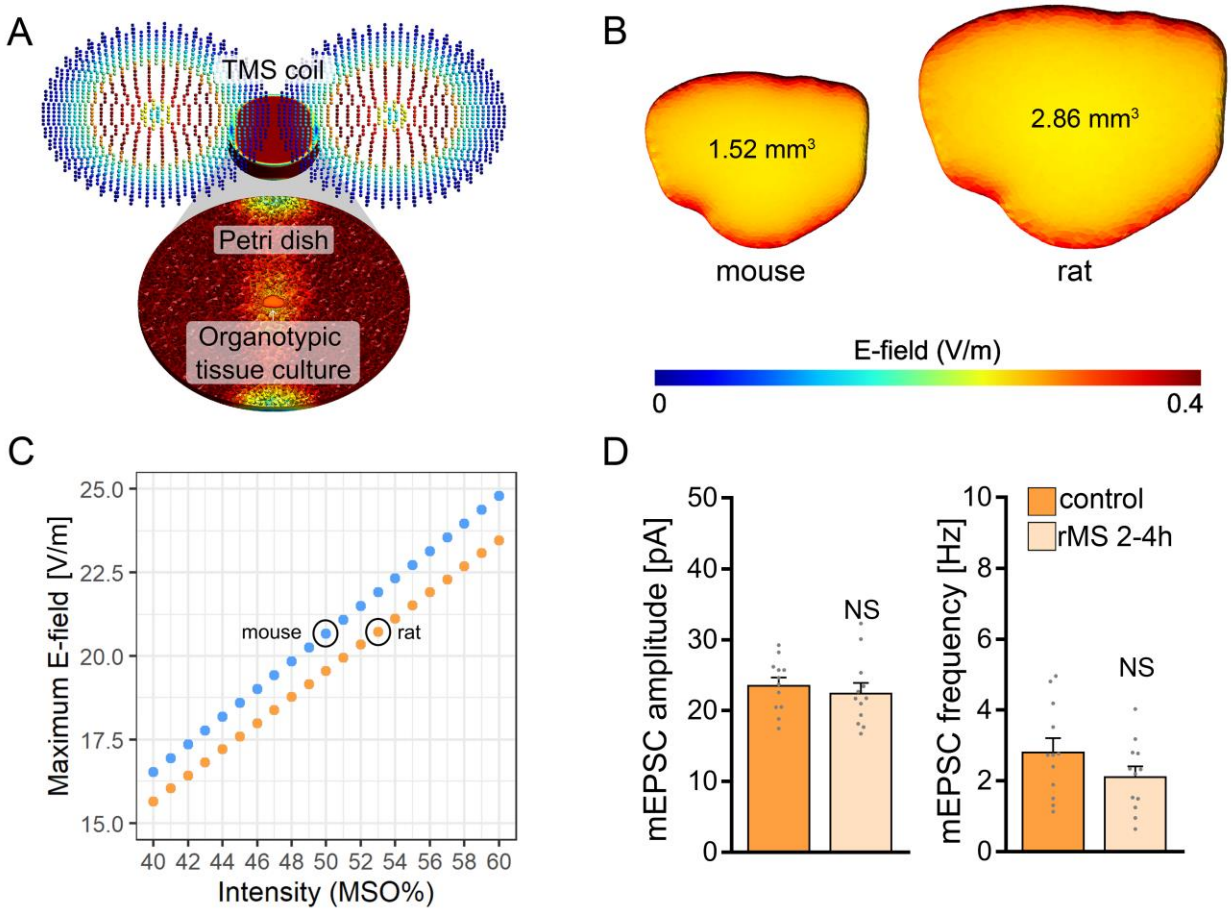

bioRxiv preprint doi: https://doi.org/10.1101/2023.09.25.559399; this version posted September 27, 2023. The copyright holder for this preprint (which was not certified by peer review) is the author/funder. All rights reserved. No reuse allowed without permission.

Figure 4

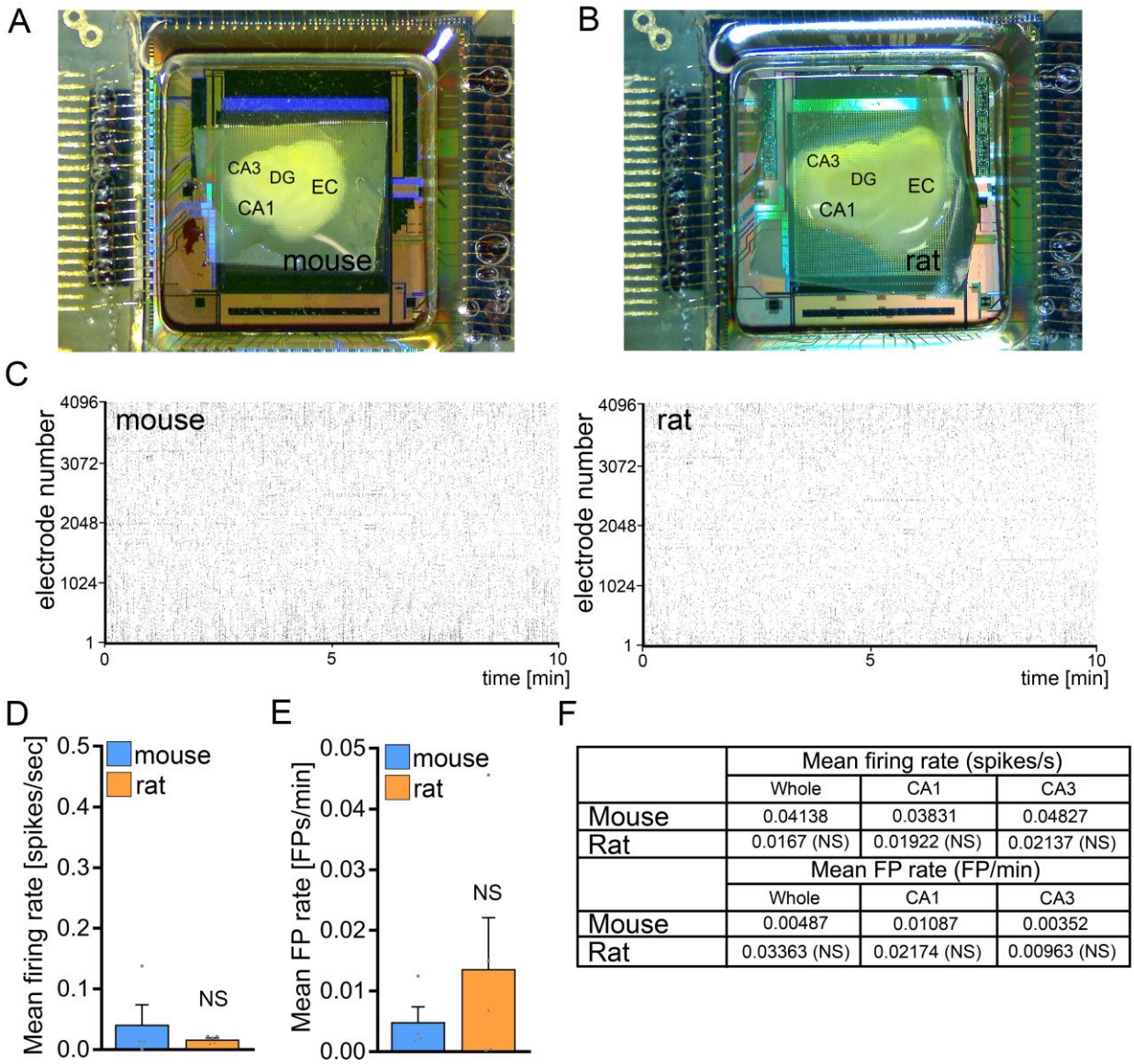

F

	Mean firing rate (spikes/s)		
	Whole	CA1	CA3
Mouse	0.04138	0.03831	0.04827
Rat	0.0167 (NS)	0.01922 (NS)	0.02137 (NS)
	Mean FP rate (FP/min)		
	Whole	CA1	CA3
Mouse	0.00487	0.01087	0.00352
Rat	0.03363 (NS)	0.02174 (NS)	0.00963 (NS)

bioRxiv preprint doi: https://doi.org/10.1101/2023.09.25.559399; this version posted September 27, 2023. The copyright holder for this preprint (which was not certified by peer review) is the author/funder. All rights reserved. No reuse allowed without permission.

Figure 5

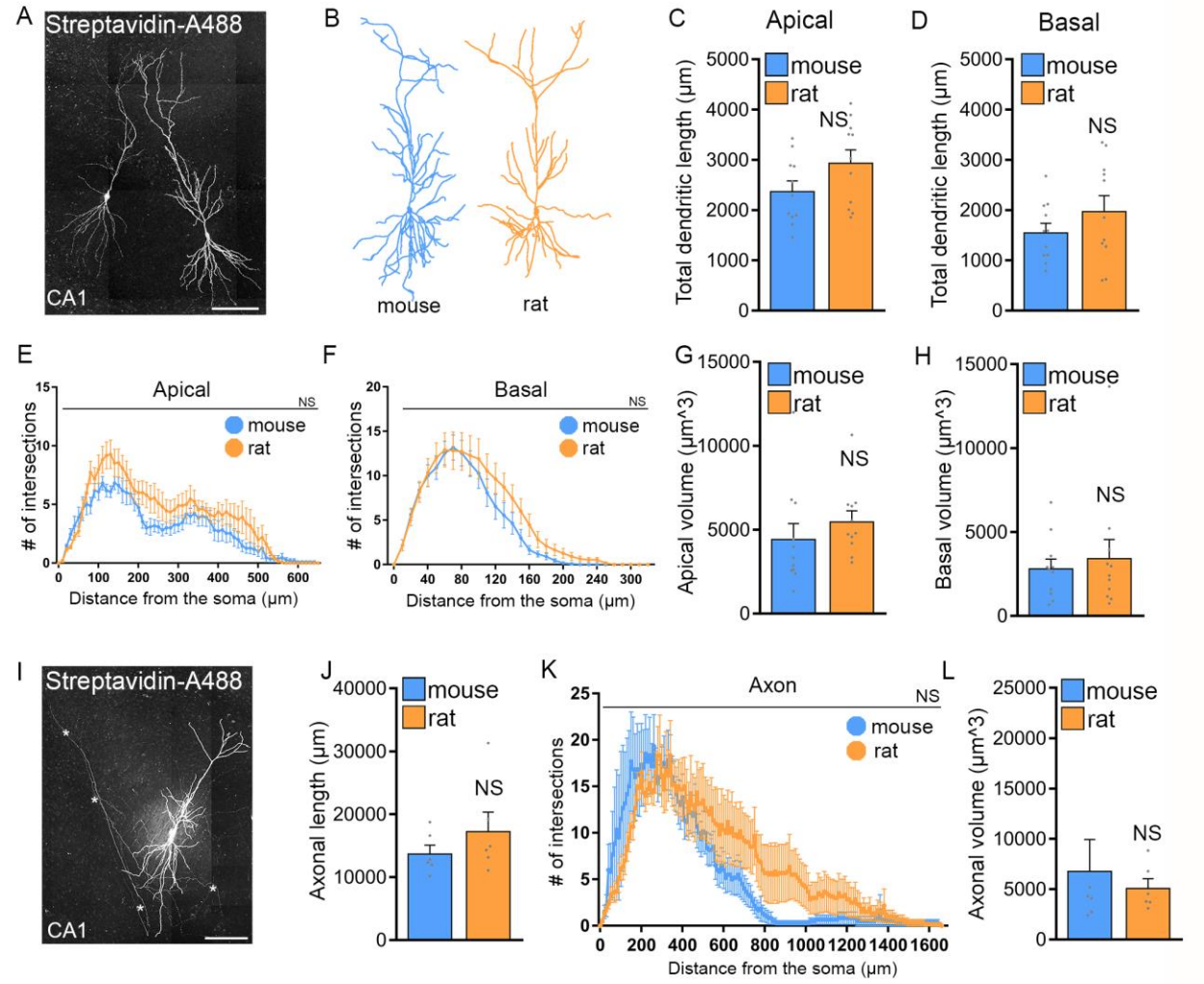

bioRxiv preprint doi: https://doi.org/10.1101/2023.09.25.559399; this version posted September 27, 2023. The copyright holder for this preprint (which was not certified by peer review) is the author/funder. All rights reserved. No reuse allowed without permission.

Figure 6

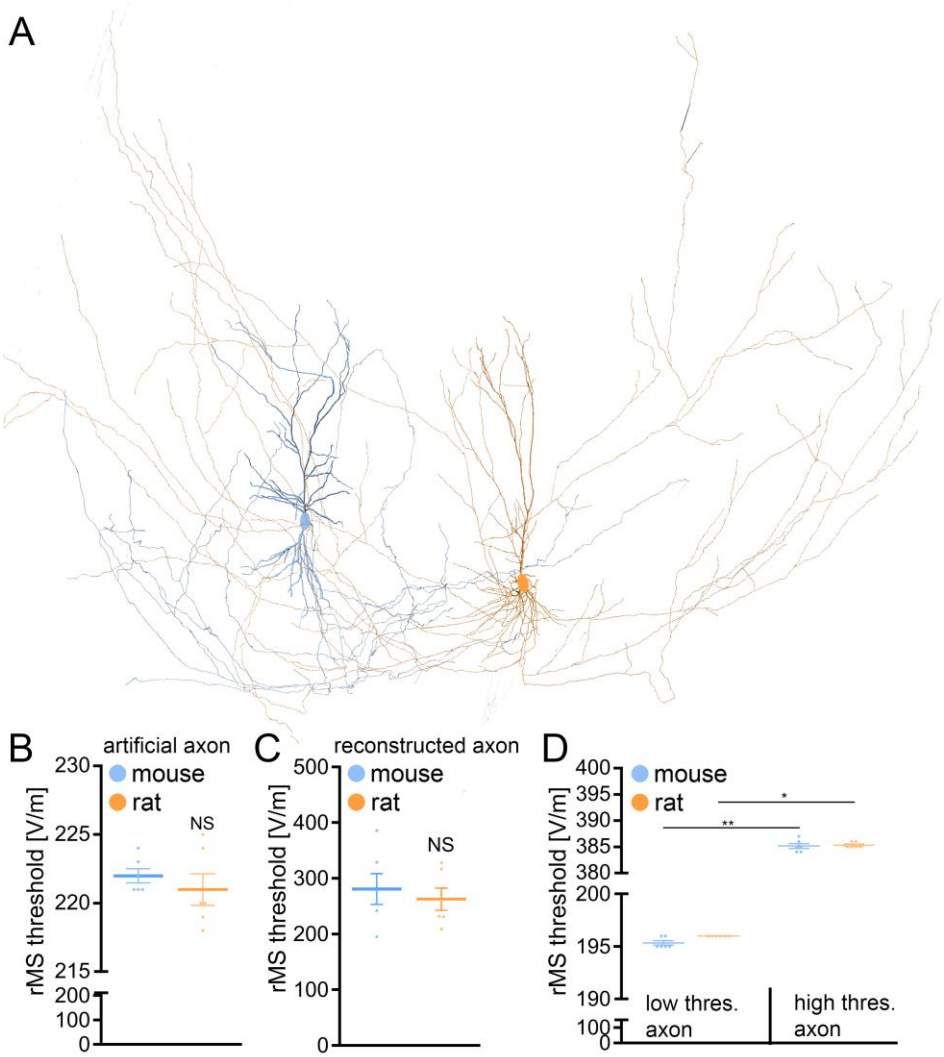

bioRxiv preprint doi: https://doi.org/10.1101/2023.09.25.559399; this version posted September 27, 2023. The copyright holder for this preprint (which was not certified by peer review) is the author/funder. All rights reserved. No reuse allowed without permission.

Figure 7

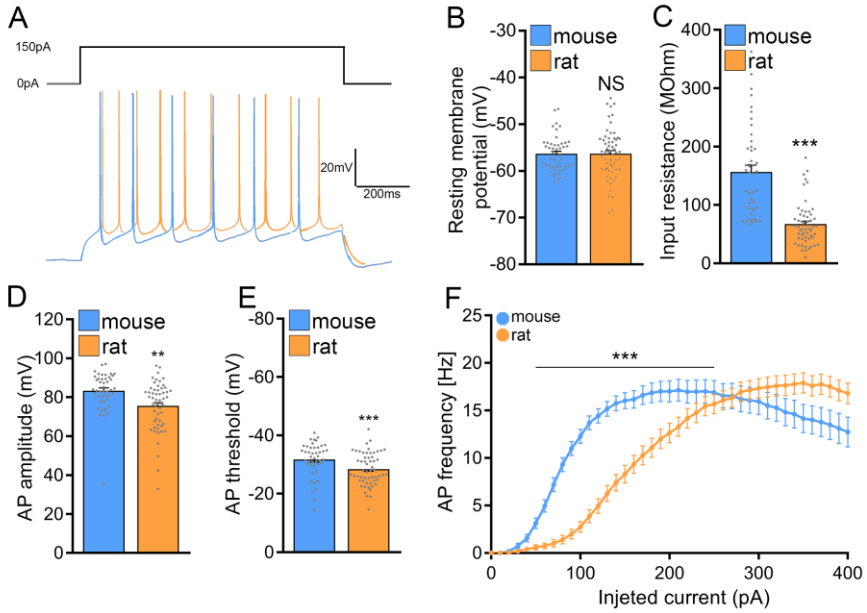

bioRxiv preprint doi: https://doi.org/10.1101/2023.09.25.559399; this version posted September 27, 2023. The copyright holder for this preprint (which was not certified by peer review) is the author/funder. All rights reserved. No reuse allowed without permission.

Figure 8